Rtf1 HMD domain facilitates global histone H2B monoubiquitination and regulates morphogenesis and virulence in the meningitis-causing pathogen *Cryptococcus neoformans*

Yixuan Jiang[1,4], Ying Liang[1,4], Fujie Zhao[1], Zhenguo Lu[1], Siyu Wang[1], Yao Meng[1], Zhanxiang Liu[1], Jing Zhang[1]*, Youbao Zhao[1,2,3]*

1 College of Veterinary Medicine, Henan Agricultural University, Zhengzhou, Henan 450046, China

2 Key Laboratory of Quality and Safety Control of Poultry Products, Ministry of Agriculture and Rural Affairs, Zhengzhou, Henan 450046, China

3 Henan Province Key Laboratory of Animal Food Pathogens Surveillance, Zhengzhou, Henan 450046, China

4 These authors contribute equally.

*Corresponding to: zhangjing@henau.edu.cn and zhaoyoubao@henau.edu.cn

Abstract

Rtf1 is generally considered to be a subunit of the Paf1 complex (Paf1C), which is a multifunctional protein complex involved in histone modification and RNA biosynthesis at multiple stages. Rtf1 is stably associated with the Paf1C in *Saccharomyces cerevisiae*, but not in other species including humans. Little is known about its function in human fungal pathogens. Here, we show that Rtf1 is required for facilitating H2B monoubiquitination (H2Bub1), and regulates fungal morphogenesis and pathogenicity in the meningitis-causing fungal pathogen *Cryptococcus neoformans*. Rtf1 is not tightly associated with the Paf1C, and its histone modification domain (HMD) is sufficient to promote H2Bub1 and the expression of genes related to fungal mating and filamentation. Moreover, Rtf1 HMD fully restores fungal morphogenesis and pathogenicity; however, it fails to restore defects of thermal tolerance and melanin production in the *rtf1*Δ strain background. The present study establishes a role for cryptococcal Rtf1 as a Paf1C-independent regulator in regulating fungal morphogenesis and pathogenicity, and highlights the function of HMD in facilitating global H2Bub1 in *C. neoformans*.

Keywords: Rtf1; histone modification domain; H2B ubiquitination; *Cryptococcus neoformans*; yeast-to-hypha transition; virulence

1. Introduction

In eukaryotes, gene transcription is regulated by dynamic changes in chromatin. The posttranslational modifications of core histones, including acetylation, methylation, and ubiquitination, represent major mechanisms by which cells alter the chromatin structural properties and regulate gene transcription [1, 2]. Among them, the monoubiquitination of a lysine (K) residue on the C-terminal of histone H2B (H2Bub1) is a conserved modification that occurs on H2B K120 residue in *Homo sapiens* and K123 residue in *Saccharomyces cerevisiae* [3, 4]. H2Bub1 is enriched at regions of active transcription but plays roles in both gene activation and repression [5-7]. In addition, H2Bub1 is required for di- and trimethylation of H3 K4 and H3 K79, subsequently modulating chromatin accessibility [8-12].

The ubiquitin conjugase (E2) Rad6 and the ubiquitin ligase (E3) Bre1 are responsible for H2Bub1 in *S. cerevisiae* [13-15]. In addition, H2Bub1 is regulated by additional factors in yeast and other eukaryotes, among which the conserved polymerase-associated factor 1 (Paf1) complex (Paf1C) is the prominent one [4, 16-19] Paf1C is a multi-functional protein complex, which impacts RNA synthesis at multiple stages [20-28]. Paf1C consists of the subunits Paf1, Ctr9, Cdc73, Rtf1, and Leo1, and the five subunits are stably associated within the complex in *S. cerevisiae* [22, 29-31]. In contrast, Rtf1 appears not to be stably associated with Paf1C in

50 human cells, despite the Paf1C is structurally and functionally conserved [32-34]. Interestingly,
51 the histone modification domain (HMD) within Rtf1 is both necessary and sufficient for
52 stimulating H2Bub1 in yeast [4, 18]. Expression of the Rtf1 HMD alone restores H2Bub1 levels
53 in *S. cerevisiae* mutants deleted for the *RTF1* gene or all five Paf1C subunits-encoding genes [3,
54 4, 18]. These studies show that Rtf1 is the only Paf1C subunit that is strictly required for
55 deposition of H2Bub1 in vivo. However, little is known about its role in human fungal
56 pathogens.

57 *Cryptococcus neoformans*, the top-ranked fungus in the WHO fungal pathogen priority
58 list, is a globally distributed opportunistic fungal pathogen that can cause life-threatening
59 cryptococcosis [35, 36]. The mortality rate of cryptococcosis is alarmingly high, especially in
60 patients with HIV infection, in whom it ranges from 41% to 61% [37, 38]. *C. neoformans* can
61 be classified into two serotypes: the serotype A *C. neoformans* and the serotype D *C.*
62 *deneoformans*. Both *C. neoformans* and *C. deneoformans* undergo yeast-to-hypha transition
63 under inducing conditions, which has been shown to be associated with fungal virulence [39,
64 40]. Thus, deciphering the regulatory mechanisms on fungal morphogenesis and pathogenesis in
65 *C. neoformans* is critical for comprehensive understanding of the nature of pathogen and
66 combating against cryptococcal infection.

67 In our previous study, we characterized the subunits of complex-associated with Set1
68 (COMPASS) and found that COMPASS-mediated H3K4 methylation (H3K4me) affects yeast-
69 to-hypha transition and virulence in both *C. neoformans* and *C. deneoformans* [41]. We also
70 preliminarily showed that H2Bub1 is required for COMPASS-mediated H3K4me by deletion of
71 *RAD6* and *RTF1* in *C. neoformans* and *C. deneoformans* [41]. However, the Here, we set out to
72 characterize the roles of Rtf1 in facilitating global H2Bub1 and to gain comprehensive insights
73 into the epigenetic regulation on fungal morphogenesis and pathogenesis in the human fungal
74 pathogen *C. neoformans*.

75 2. Materials and methods

76 *2.1. Strains, culture conditions, and microscopy examination*

77 Strains used in this study are listed in the Supplemental Table S1. *C. deneoformans* and
78 *C. neoformans* strains were maintained on YPD medium unless specified otherwise.
79 Transformants obtained from transient CRISPR-Cas9 coupled with electroporation (TRACE)
80 were selected on YPD medium with 100 μg/mL of nourseothricin, 100 μg/mL of G418, or
81 200 μg/mL of hygromycin.

82 Strains for phenotypic assays were grown overnight in liquid YPD medium at 30°C
83 with shaking. The cells were washed with sterile water, adjusted to an optical density at 600 nm
84 (OD_{600}) of 3.0, and serially diluted. For filamentation tests, aliquots (3 μL) of cell suspensions
85 (OD_{600} = 3.0) were spotted onto V8 plates and cultured at room temperature in the dark. For
86 morphological examinations, all strains were examined under a stereoscope. For spotting
87 assays, aliquots (3 μL) of serial dilutions starting from OD_{600} = 3.0 were spotted onto agar
88 medium with supplements and cultured under the noted conditions.

89 ***2.2. Gene manipulation***

90 Cryptococcal genes were deleted following the TRACE protocol [42, 43]. In brief, a
91 deletion construct with approximately 1 kb of homologous arms flanking a target gene and the
92 dominant marker was cloned through fusion PCR. This construct was mixed with PCR products
93 of *CAS9* and a relevant guide RNA (gRNA), and the mixture was introduced into recipient
94 strains by electroporation as described previously [43]. Resulting yeast colonies were screened
95 by two rounds of diagnostic PCR. The first round of PCR was performed to detect the
96 integration of the construct into the corresponding locus of the target gene. The second round of
97 PCR was performed to confirm knockout of the target fragment. All primers used to make gene
98 deletion mutants are listed in the Supplemental Table S1.

99 For gene complementation, the ORFs plus approximately 1.0 kb of their upstream
100 regions were amplified by PCR and cloned into vectors through T5 exonuclease-dependent
101 assembly as previously described [44]. For gene overexpression with inducible or constitutively
102 active promoters, the constructs were obtained by amplifying the entire ORF by PCR and
103 cloning the PCR products into vectors at the downstream of *CTR4*, *TEF1*, or *GPD1* promoter.
104 All plasmids were confirmed by restriction enzyme digestion and sequencing. The confirmed
105 constructs, together with PCR products of *CAS9* and gRNA targeting the Safe Haven locus [45,
106 46], were introduced into recipient *Cryptococcus* strains. The transformants were passaged once
107 per day for five days and cultured on selection plates to obtain stable transformants. Then, two
108 rounds of diagnostic PCR were performed to confirm the integration and orientation of
109 constructs into the Safe Haven locus. All primers and plasmids used for gene complementation
110 and overexpression are listed in the Supplemental Table S1.

111 ***2.3. Protein extraction and western blotting***

112 Proteins were extracted from *Cryptococcus* cells according to a previously described
113 method [47]. Aliquots of proteins were separated on 4%-to-12% gradient SDS-PAGE gels and
114 then transferred to a polyvinylidene difluoride membrane for Western blot analyses. Antibodies
115 used in this study are listed in the Supplemental Table S1. For co-immunoprecipitation assays

116 coupled with mass spectrometry (CoIP/MS), whole cell extracts of experimental strains were
117 incubated with FLAG-trap (Sigma) according to the manufacturer' s instructions. Proteins in the
118 eluted samples were loaded in SDS-PAGE gel, digested, and analysed by the proteome facility
119 centre of Institute of Microbiology, Chinese Academy of Sciences.

120 ***2.4. RNA extraction and qPCR assays***

121 *Cryptococcus* strains were cultured in liquid YPD with shaking at 220 rpm at 30 °C
122 overnight, or on solid V8 medium at room temperature in the dark for 24 h. The cultures were
123 collected, flash frozen in liquid nitrogen, and lyophilized for 24 h. Total RNA was isolated with
124 the PureLink RNA Mini Kit (Invitrogen), and first strand cDNA was synthesized using the
125 GoScript Reverse Transcription System (Promega) following the manufacturer's instructions.
126 The Power SYBR Green system (Invitrogen) was used for RT-PCR. All the primers used here
127 are listed in the Supplemental Table S1. Relative transcript levels were determined using the
128 ΔΔCt method as described previously. Three biological replicates were included for all tests.
129 Statistical significance was determined using a Student's t-test. Differences for which $p < 0.05$
130 were considered statistically significant.

131 ***2.5. RNA-seq and data analysis***

132 For RNA-seq analyses, strains were cultured in YPD liquid medium at 30 °C overnight.
133 The cells were washed with ddH2O and spotted on V8 medium to stimulate unisexual
134 reproduction. The level and integrity of RNA in each sample were evaluated using a Qubit RNA
135 Assay Kit on a Qubit 2.0 Fluorometer (Life Technologies, CA, USA) and RNA Nano 6000
136 Assay Kit with the Bioanalyzer 2100 system (Agilent Technologies, CA, USA), respectively.
137 RNA purity was assessed using a Nano Photometer spectrophotometer (IMPLEN, CA, USA).
138 The transcriptome libraries were generated using the VAHTS mRNA-seq v2 Library Prep Kit
139 (Vazyme Biotech Co., Ltd, Nanjing, China) according to the manufacturer's instructions.

140 The transcriptome libraries were sequenced by Annoroad Gene Technology Co., Ltd
141 (Beijing, China) on an Illumina platform. For RNA-seq analysis, the quality of sequenced clean
142 data was analyzed using FastQC software. Subsequently, sequences from approximately 2 GB
143 of clean data for each sample were mapped to the genome sequence of *C. deneoformans*
144 XL280α using STAT. Gene expression levels were measured in transcripts per million (TPM)
145 by Stringtie to determine unigenes. All unigenes were subsequently aligned against the well-
146 annotated genome of JEC21, which served as the parent strain to generate XL280α through a
147 cross with B3501α. The differential expression of genes (DEGs) was assessed using DEseq2 of
148 the R package and defined based on the fold change criterion (log2|fold-change | > 1.0, adjusted
149 p value < 0.05).

150 ***2.6. Virulence trait assays***

151 Strains for examining virulence factors were grown overnight in liquid YPD at 30 °C
152 with shaking. The overnight cultures were washed with sterile water, adjusted to OD_{600} = 3.0,
153 and serially diluted. For thermal tolerance, melanin production, and capsule formation assay on
154 solid plates, aliquots (3 μL) of serially diluted cell suspensions were spotted onto YPD plate, L-
155 dopamine media, and 10% fetal bovine serum (FBS) media [48], respectively. Thermal
156 tolerance was test at 30, 37, and 39 °C; melanin production was tested at 30 °C in the dark;
157 capsule formation was tested at 37 °C with 5% CO_2 for 48 h. The capsule was visualized by
158 staining with India ink and observed under a microscope. Images were captured using Zeiss
159 Axio Imager M2 microscope. At least 50 cells were quantified and processed in ImageJ
160 software to measure capsule and body sizes. All assays were repeated at least three times.

161 For melanin production assay in liquid media, the overnight cultures were washed with
162 sterile water, adjusted to OD_{600} = 0.3 and transferred to L-DOPA medium (containing 0.1% L-
163 asparagine, 0.1% dextrose, 3 mg/ml KH_2PO_4, 0.25 mg/ml thiamine, 5 ng/ml biotin 0.2 mg/ml
164 $MgSO_4 \cdot 7\ H_2O$ and 1 μg/ml L-DOPA). H99 strains grown for 48h at 30℃, each strain counted
165 and diluted at $2x10^7$ cells/mL, while XL280 cells was induced at 30℃ for 96h and diluted at
166 $7x10^7$ cells/mL. OD_{490} was measured to determine melanin production.

167 ***2.7. Murine models of cryptococcosis***

168 *Intranasal infection model* Female Balb/C mice of 8–10 weeks old were purchased
169 from the Laboratory Animal Center of Zhengzhou University, China. Cryptococcal strains were
170 inoculated in 3 mL of liquid YPD medium with the initial OD_{600}=0.2 (approximately 10^6
171 cell/mL) and incubated for 15 hr at 30 °C with shaking. Prior to intranasal infection, cells were
172 washed with sterile saline three times and adjusted to the final concentration of 2×10^6 cell/mL.
173 Once the mice were sedated with ketamine and xylazine via intraperitoneal injection, 50 μL of
174 the cell suspension (1×10^5 cells per mouse) were inoculated intranasally as previously described
175 [41, 49-51]. Mice were monitored daily for disease progression. Animals were euthanized at 10
176 DPI, and lungs were dissected for fungal burden quantification.

177 *Intravenous infection model* Prior to intravenous infections, cryptococcal cells were
178 washed with sterile saline three times and adjusted to the final concentration of 2×10^6 cell/mL.
179 Mice were sedated with Isoflurane. 50 μL of the cell suspension (1×10^5 cells per mouse) were
180 injected intravenously as previously described [41, 49-51]. After DPI 7, animals were
181 euthanized, and the brain, lungs, kidneys, and spleens were dissected.

182 For fungal burden quantifications, dissected organs were homogenized in 2 mL of cold
183 sterile PBS. Tissue suspensions were serially diluted in PBS and plated onto YNB agar medium
184 and incubated at 30°C for 2 days before counting the CFUs.

185 ***2.8. DAPI staining***

186 DAPI (4',6-diamidino-2-phenylindole) staining assays were performed as previously
187 described [52]. Briefly, yeast cells or hyphae were collected and fixed with 3.7% formaldehyde
188 and permeabilized in 1% Triton X-100. The cells were then washed three times with PBS and
189 incubated in 2 μg/mL DAPI before being dropped onto a glass slide for fluorescent microscopic
190 observation.

191 ***2.9. Data availability***

192 All RNA-seq data are going to be available at the NCBI (SUB14425795).

193 **3. Results**

194 ***3.1. Rtf1-mediated global H2Bub1 regulates cryptococcal yeast-to-hypha***
195 ***transition***

196 PAF1C subunit Rtf1 functions at the interface between Paf1C and Rad6/Bre1, and is
197 required for deposition of H2Bub1 in all the eukaryotic species examined [53]. We showed that
198 Rtf1 is also required for H2Bub1 and subsequent COMPASS-mediated H3K4me in the *C.*
199 *deneoformans* reference strain XL280α background (Figure 1A and B) [41]. Interestingly, loss
200 of H2Bub1 through deleting *RTF1* blocked unisexual yeast-to-hypha transition in *C.*
201 *deneoformans* (Supplementary Figure S1A) [41]. To establish the role of Rtf1 in regulating
202 cryptococcal filamentation during bisexual mating, we obtained *RTF1* deletion mutant in the *C.*
203 *deneoformans* reference strain XL280**a** background through spore dissection from cross
204 between *rtf1*Δα and XL280**a**, and conducted bisexual cross assay under mating-inducing
205 condition on V8 media. The mating hyphae during unilateral mating between *rtf1*Δα and
206 XL280**a** were produced at a slightly reduced level compared to mating between reference
207 partners XL280α and XL280**a**, while filamentation was significantly reduced during bilateral
208 mating between *rtf1*Δα and *rtf1*Δ**a** (Figure 1C).

209 During bisexual mating in *C. deneoformans*, mating pheromone (MF) is produced in
210 cells and secreted through the transporter Ste6 [54]. Secreted pheromone induces mating
211 response by binding to the compatible receptor on the cell surface of opposite mating type (Mf**a**
212 to Ste3α or Mfα to Ste3**a**) [55, 56]. In addition, Mat2, which is a direct downstream

213 transcription factor of the Cpk1 MAPK pathway, regulates the transcription of genes encoding
214 the above-mentioned pheromone sensing proteins [57] (Figure 1D). Given the bisexual mating
215 hyphae reduction caused by *RTF1* deletion, we further investigated the effects of *RTF1* deletion
216 on genes involved in bisexual mating at transcript level via qPCR. In comparison to the mating-
217 suppressing condition (YPD media), the transcript levels of *MAT2*, *MFα2*, *STE6*, and *STE3α*
218 were all highly induced under mating-inducing condition (V8 media). However, these
219 inductions were significantly impaired by deletion of *RTF1* (Figure 1D). These results strongly
220 indicated that Rtf1 facilitates H2Bub1 and regulates the expression of genes involved in fungal
221 morphogenesis in *C. deneoformans*.

222 *3.2. Ectopic expression of HMD restores global H2Bub1 levels and cryptococcal*
223 *yeast-to-hypha transition*

224 As the key subunit of Paf1C in mediating histone H2Bub1, Rtf1 is conserved across
225 eukaryotes and consists of two conserved domains, a histone modification domain HMD and a
226 domain that contains three highly conserved positively charged residues (Plus3) (Figure 1E). It
227 is worth noting that Rtf1 protein and Plus3 domain in *C. neoformans* is evolutionally close to
228 higher eukaryotes, such as *H. sapiens* and *Drosophila melanogaster* (Figure 1F and
229 Supplementary Figure S1B and C), while the HMD domain is distant from higher eukaryotes
230 (Figure 1G). To further dissect the roles of Rtf1 HMD and Plus3 in facilitating histone H2Bub1
231 in *C. deneoformans*, we constructed the truncated versions of Rtf1 that encode HMD (53-145)
232 or Plus3 (227-333) with a nuclear localization sequence (NLS) added in their N terminus,
233 respectively, driven by the constitutive promoter and tagged with FLAG (Figure 1H).
234 Interestingly, overexpression of HMD domain itself significantly promoted H2Bub1 to an even
235 higher level in the *rtf1*Δ strain, compared to that in WT strain and the strain overexpressing the
236 full length of *RTF1* (Figure 1I), while overexpression of the Plus3 failed to restore H2Bub1
237 (Figure 1I). These results demonstrated that HMD alone is sufficient to facilitate the global
238 H2Bub1 level in *C. deneoformans*.

239 Our previous studies have demonstrated that H2Bub1 is positively related to the
240 filamentation in *C. neoformans* [41]. Consistently, overexpressing either the full length of *RTF1*
241 or the HMD domain, but not Plus3, promoted the filamentation in *rtf1*Δ strain (Figure 1J). To
242 gain an overview of effects on gene expression patterns by the overexpression of HMD domain,
243 we conducted transcriptome profiling by RNA-seq under filamentation-inducing condition (on
244 V8 media). The results showed that the expression levels of 668 genes were significantly
245 changed due to the *RTF1* deletion compared to the WT on V8 media ($|\log2FC| > 1$, adjusted P
246 value < 0.05), with 308 genes significantly upregulated and 360 genes downregulated (Figure
247 2A, Supplementary Data S1). It is worth noting that the downregulated genes are mainly

248 enriched in GO categories related to sexual reproduction, pheromone-dependent signaling, and
249 filamentous growth (Supplementary Figure S2). Strikingly, overexpression of HMD domain
250 alone in *rtf1*Δ strain successfully restored the expression of these genes to similar levels as those
251 in wild-type XL280 strain, while overexpression of Plus3 domain failed to do so (Figure 2A). In
252 particular, the expression levels of marker genes of filamentous growth (*ZNF2* and *CFL1*) [57,
253 58]and genes involved in sexual reproduction and pheromone-dependent signaling (*MFα*,
254 *STE3α*, and *STE6*) as shown in Figure 1D were restored by overexpressing HMD domain alone
255 in the rtf1Δ background (Figure 2B, Supplementary Figure S3). These findings from
256 transcriptome analyses were further confirmed by qPCR (Figure 2C). In addition, the
257 downregulated genes in *rtf1*Δ/Plus3 cells were significantly enriched in common GO categories
258 as the downregulated genes in *rtf1*Δ cells (Supplementary Figure S2), relative to the wild-type
259 XL280 strain. Together, these results strongly suggested that HMD domain is sufficient to
260 facilitate global H2Bub1 to promote expression of genes associated with filamentation.

261 ***3.3. HMD is sufficient to facilitate global H2Bub1 and the consequent yeast-to-***
262 ***hypha transition***

263 The full length Rtf1 or HMD domain should properly translocate into the nucleus to
264 facilitate histone H2Bub1. To confirm the function of Rtf1 and HMD domain in facilitating
265 H2Bub1, we artificially intervened their sub-cellular localizations and evaluated the effects of
266 non-nuclear (cell membrane) and nuclear localizations on H2Bub1, H3K43me, and
267 filamentation. To achieve cell membrane localization, we fused the full length Rtf1 and HMD
268 with a cell membrane RGS2-mNeonGreen tag [59, 60] (Figure 3A), and introduced the
269 constructs into the *rtf1*Δ strain, respectively. As indicated by the mNeonGreen fluorescence,
270 HMD domain and the originally nuclear-localized full length Rtf1 translocated to cell
271 membrane after fusing with the RGS2-mNeongreen tag (Figure 3B). Both nuclear-localized
272 Rtf1 and HMD domain restored the levels of H2Bub1, H3K4me, and filamentation (Figure 3C
273 and D). In contrast, the non-nuclear-localized full length Rtf1 or HMD domain failed to restore
274 the levels of H2Bub1, H3K4me, or filamentation in the *rtf1*Δ strain (Figure 3C and D). These
275 results further supported the role of Rtf1 HMD domain in facilitating H2Bub1.

276 Rtf1 HMD domain is conserved from various eukaryotic species, and the residue of
277 glutamine at position 95 (E95, Figure 3E, F and G) has been shown to be critical for the
278 function of Rtf1 [28]. It is noteworthy that the residue of phenylalanine at position 118 (F118)
279 in *C. neoformans* is as conserved as the residue in *S. cerevisiae* (Figure 3E), which is critical for
280 H2Bub1 in yeast, although it is not conserved in other eukaryotic species [28]. To investigate
281 their roles in cryptococcal Rtf1 HMD domain, we constructed site-mutated alleles of full length
282 Rtf1 ($Rtf1^{E95A}$ and $Rtf1^{F118A}$) and HMD domain (HMD^{E95A} and HMD^{F118A}) and introduced them

283 into the *rtf1*Δ strain, respectively. Both Rtf1^{E95A} and HMD^{E95A} failed to restored H2Bub1 and
284 H3K4me levels in the *rtf1*Δ strain, while Rtf1^{F118A} and HMD^{F118A} partially restored H2Bub1 and
285 H3K4me levels (Figure 3H). In consistent with the histone modification outputs, the mutants
286 expressing Rtf1^{E95A} or HMD^{E95A} showed non-filamentous phenotypes similar as the staring
287 *rtf1*Δ strain, while mutants expressing Rtf1^{F118A} or HMD^{F118A} produced more filaments than the
288 starting *rtf1*Δ strain (Figure 3I). Together, these results demonstrated that Rtf1 HMD domain
289 itself is sufficient to facilitate H2Bub1 and consequent cryptococcal filamentation with E95 as a
290 critical conserved residue.

291 ***3.4. Roles of the global H2Bub1 level in cryptococcal virulence factor***
292 ***production***

293 To investigate the role of HMD-mediated H2Bub1 in cryptococcal virulence, we
294 constructed *RTF1* deletion strain and mutants overexpressing the full length Rtf1, HMD
295 domain, Plus3 domain, or mutated alleles of Rtf1^{E95A} and HMD^{E95A}, respectively, in the
296 clinically isolated serotype A *C. neoformans* H99 strain background. Consistent with what we
297 observed in the serotype D *C. deneoformans*, deletion of *RTF1* abolished H2Bub1 and
298 H3K4me, and overexpressing the full length of Rtf1 and HMD domain alone, but not the Plus3
299 domain, Rtf1^{E95A} or HMD^{E95A}, successfully restored H2Bub1 and H3K4me (Figure 4A). Next,
300 we investigated whether Rtf1 HMD domain is involved in the production of major virulence
301 factors in vitro and pathogenicity in murine models of cryptococcosis. As shown in Figure 4B,
302 the *rtf1*Δ mutant had severe growth defect at 39°C, and overexpression of the full length Rtf1,
303 but not the Plus3 domain, Rtf1^{E95A} or HMD^{E95A}, partially restored the thermal sensitivity of the
304 *rtf1*Δ mutant (Figure 4B). Interestingly, overexpression of HMD domain alone restored the
305 growth defect of *rtf1*Δ mutant at 39°C to a level that was worse than the expression of the full
306 length of Rtf1 (Figure 4B). Furthermore, the *rtf1*Δ mutant was incapable to produce melanin,
307 and only the full length of Rtf1 restored its melanin production, while the HMD domain alone
308 failed to do so (Figure 4B). These results strongly indicate that the full length of Rtf1, but not
309 only the levels of global H2Bub1, is required to regulate thermal tolerance and melanin
310 production in *C. neoformans*.
311 Capsule production and cell size are known factors that are tightly associated with
312 cryptococcal virulence. We tested the capsule production in *RTF1*-related mutants on the FBS
313 solid media cultured at 37 °C with 5% CO_2. The control mutant strain *nrg1*Δ produced no
314 capsule under this condition, and the *rtf1*Δ mutant produced slightly less capsule compared to
315 the wild-type H99 strain in terms of capsule thickness (Figure 4C). Interestingly, the cell size of
316 the *rtf1*Δ mutant were significantly larger than the H99 strain under this condition (Figure
317 4C&D), and only overexpression of the full length of Rft1 restored the cell size enlargement

318 phenotype (Figure 4D). Consistently, the ratio between diameters of capsule layer and cell body
319 in *rtf1*Δ was significantly smaller than the ratio in the H99 strain (Figure 4E). In addition,
320 overexpression of the full length Rtf1 partially restored the ratio to the level as in the H99 strain,
321 and the HMD, Plus3, Rtf1^{E95A} or HMD^{E95A} failed to do so (Figure 4E). These results
322 showed that the global distribution of H2Bub1 across the chromosome play critical
323 roles in regulating capsule production and cell size in *C. neoformans*.

324 We further investigated the effects of Rtf1 on virulence traits in *C. deneoformans*.
325 Given the poor growth of serotype D strains under higher temperature, we only determined the
326 production of melanin and capsule in *C. deneoformans* strains. Consistent with what we
327 observed in *C. neoformans* H99 strain background, the *rtf1*Δ mutant produced less melanin in
328 L-DOPA media, and overexpression of the full length Rtf1 restored the melanin production and
329 the HMD domain failed to do so (Figure 4F). In addition, the cell size and ratio between
330 diameters of capsule layer and cell body in *rtf1*Δ were significantly smaller than the those in the
331 XL280 reference strain (Figure 4G&H). Overexpression of the full length Rtf1 partially restored
332 the ratio to the level as in the XL280 strain, while overexpression the HMD, failed to do so
333 (Figure 4H). Surprisingly, overexpression of the Plus3 domain, Rtf1^{E95A} or HMD^{E95A} partially
334 restored the melanin production and the ratio between diameters of capsule layer and cell body
335 in the *rtf1*Δ mutant in *C. deneoformans* (Figure 4F&H). These results indicated that Rtf1 protein
336 may have serotype-specific regulatory mode-of-actions in *C. neoformans* and *C. deneoformans*
337 regarding to melanin and capsule production.

338 *3.5. Roles of the HMD-mediated H2Bub1 in regulating cryptococcal*
339 *pathogenicity*

340 To further investigate the role of HMD-mediated H2Bub1 in the pathogenicity of *C.*
341 *neoformans*, we tested the fungal burdens and survival rates of wild-type, *rtf1*Δ, and
342 complemented strains in intranasal and intravenous murine models of cryptococcosis (Figure
343 5A). Our results showed that both intranasally and intravenously infected lungs by the *rtf1*Δ
344 mutant had significantly reduced fungal burden compared to lungs infected by wild-type, full
345 length *RTF1*-complemented, or HMD-complemented strains (Figure 5B and C). The lungs
346 infected by Plus3-, Rtf1^{E95A}- or HMD^{E95A}-complemented strain had comparable fungal burden
347 relative to the *rtf1*Δ-infected lungs (Figure 5B and C). Similar trends in effects on fungal burden
348 were observed in other intravenously infected organs, including brain, kidney, and spleen
349 (Figure 5D, E and F). In consistent with the fungal burden analysis, the pathogenicity of *rtf1*Δ
350 mutant in the intravenous model of cryptococcosis were significantly attenuated compared to
351 the wild-type strain and strains complemented with the full length of Rtf1 or the HMD domain,
352 while the Plus3, Rtf1^{E95A}, or HMD^{E95A} failed to complement the attenuated virulence of the

353 *rtf1*Δ mutant (Figure 5G). Together, our findings suggest that HMD-mediated H2Bub1 is
354 essential for the successful survival and proliferation of *C. neoformans* during infection.

355 **4. Discussion**

356 In this study, we investigated the role of Rtf1 in promoting H2Bub1 and consequently
357 regulating cryptococcus yeast-to-hypha transition and virulence. Here, we demonstrated that the
358 global H2Bub1 plays pleiotropic roles in the sexual reproduction, morphogenesis, melanin
359 production, thermal tolerance, and pathogenicity of *C. deneoformans* and *C. neoformans*.
360 Interestingly, the Rtf1 HMD domain alone is sufficient to facilitate global H2Bub1 and
361 subsequent H3K4me. The HMD domain could fully restore the deficiencies on filamentation in
362 vitro and pathogenicity in a murine model of cryptococcosis. Our results fit a model in which
363 Rtf1 facilitates the global H2Bub1 and subsequent H3K4me levels, in order to promote
364 expression of genes involved in morphogenesis and pathogenicity in *C. neoformans*.

365 Paf1C was first identified as the RNA polymerase II transcriptional regulator
366 functioning in transcription elongation, and is also required for Rad6/Bre1-mediated H2Bub1
367 and subsequent H3K4me. Whether and how these two roles interplay with each other remain
368 unclear. In yeast, Paf1C contains five highly conserved core subunits Paf1, Leo1, Ctr9, Cdc73,
369 and Rtf1, which is stably associated with the other subunits within Paf1C. However, the human
370 core Paf1C was shown to interact with RNA polymerase II, in the absence of human Rtf1
371 homolog, indicating the dispensable role of human Rtf1 in the function of Paf1C [61]. The
372 Paf1C is conserved and consists of five subunits in *C. neoformans* [41]. To investigate the
373 association of Rtf1 with Paf1C in *C. neoformans*, we conducted co-immunoprecipitation
374 coupled with mass spectrometry (CoIP/MS) assays. None of the other four Paf1C subunits
375 could be detected with either FLAG-tagged full length of Rtf1, HMD, or Plus3 as bait
376 (Supplementary Data S2), strongly indicating that Rtf1 is not stably associated with the Paf1C
377 in *C. neoformans*.

378 Rtf1 is critical for H2Bub1 levels, and its deletion abolishes global H2Bub1 in both
379 yeast and humans. It is reasoned that Rtf1 may play dual roles in regulating elongation of gene
380 transcription and deposition of H2Bub1. To gain a comprehensive insight into the function of
381 Rtf1 in eukaryotes, we investigated the role of Rtf1 in human fungal pathogens *C.*
382 *deneoformans* and *C. neoformans* that belong to Basidiomycota. Besides its conserved functions
383 in facilitating global H2Bub1, we also found it is required for fungal morphogenesis and
384 pathogenicity. We showed that HMD domain alone is sufficient to restore cryptococcal
385 filamentation and virulence (Figure 1, 3 and Figure 5), concomitant with the restoration of
386 global H2Bub1 levels (Figure 1, 3 and 4). Given that HMD domain alone lacks regions of full
387 length Rtf1 required for its interactions with other Paf1C subunits and transcribed regions of

genes [4, 62], our results on the HMD domain support for a model in which the function of Rtf1 in regulating H2Bub1 is uncoupled from interaction with other subunits of Paf1C, and it is required for cryptococcal development and virulence (Figure 5H). Biochemical and biophysical studies on the association of Rtf1 with Paf1C subunits and Rad6/Bre1 would provide further insights into its mode of action in regulating establishment and deposition of H2Bub1.

Rtf1 contains two conserved domains Plus3 and HMD (Figure 1E). The Plus3 domain has been shown to interact with single-stranded DNA, indicating a role for Rtf1 in the elongation bubble during transcription elongation [62]. In addition, Plus3 may also function in facilitating proper positioning of H2Bub1, especially in regions of actively transcribed genes [4]. Here, we showed that the Plus3 domain alone has no effects on global H2Bub1, while the HMD domain alone could facilitate H2Bub1 (Figure 1A). Moreover, the *rtf1*Δ mutant showed reduced thermal tolerance with growth defects at 37°C and 39°C, compared to the wild-type strain (Figure 4C). The full length of Rtf1 or HMD domain alone fully restored the growth defect of *rtf1*Δ mutant at 37°C; However, both of them only partially restored the growth defect at 39°C (Figure 4C). In addition, only the full length of Rtf1 restored melanin production in the *rtf1*Δ mutant (Figure 4D), although the HMD domain alone fully restored the global H2Bub1 levels in *C. neoformans* (Figure 4A). There are two possibilities that may lead to these observations: (1) H2Bub1 was not properly depositioned with expression of only HMD domain, although the global level of H2Bub1 seems normal; (2) production of the virulence factors may require functions of Rtf1 and/or Paf1C in transcription elongation, which is absent in HMD-complemented strain [4, 18]. These results on the HMD domain in regulating virulence factors provide insights into the function of full-length Rtf1 and interactions with other subunits of Paf1C. A detailed comparison of H2Bub1 occupancies across chromosomes between cells expressing the full length of Rtf1 and HMD alone would be of great interest. In addition, overexpression of truncated version of Rtf1 in serotype A and D background *rtf1*Δ mutants give different output in terms of melanin and capsule production. These unexpected findings indicate that the Rtf1 protein may have different regulatory function in serotype A and D strains, in addition to the shared function in mediating H2Bub1. Further studies are required to uncover the roles of Paf1C and Rtf1 in facilitating proper deposition of H2Bub1 to regulate fungal morphogenesis and pathogenicity.

Acknowledgements

We thank the Zhao lab for their continued interest and ideas. We thank the Big Data Center and Bioinformatics Center at Department of Veterinary Medicine, Henan Agricultural University for providing high performance computing service. This work was supported by

National Natural Science Foundation of China (no. 32373093 and 30900880 to Zhao Y; 32402947 to Zhang J) and Henan Agricultural University (no. 30500946 to Zhao Y).

Disclosure statement

No potential conflict of interest was reported by the author(s).

References

1. Taylor, B.C. and N.L. Young, *Combinations of histone post-translational modifications.* Biochemical Journal, 2021. **478**(3): p. 511-532.
2. Yun, M., et al., *Readers of histone modifications.* Cell Res, 2011. **21**(4): p. 564-78.
3. Fetian, T., et al., *Paf1 complex subunit Rtf1 stimulates H2B ubiquitylation by interacting with the highly conserved N-terminal helix of Rad6.* Proc Natl Acad Sci U S A, 2023. **120**(22): p. e2220041120.
4. Piro, A.S., et al., *Small region of Rtf1 protein can substitute for complete Paf1 complex in facilitating global histone H2B ubiquitylation in yeast.* Proc Natl Acad Sci U S A, 2012. **109**(27): p. 10837-42.
5. Batta, K., et al., *Genome-wide function of H2B ubiquitylation in promoter and genic regions.* Genes Dev, 2011. **25**(21): p. 2254-65.
6. Sun, Z.W. and C.D. Allis, *Ubiquitination of histone H2B regulates H3 methylation and gene silencing in yeast.* Nature, 2002. **418**(6893): p. 104-8.
7. Briggs, S.D., et al., *Gene silencing: trans-histone regulatory pathway in chromatin.* Nature, 2002. **418**(6897): p. 498.
8. Worden, E.J. and C. Wolberger, *Activation and regulation of H2B-Ubiquitin-dependent histone methyltransferases.* Curr Opin Struct Biol, 2019. **59**: p. 98-106.
9. Dover, J., et al., *Methylation of histone H3 by COMPASS requires ubiquitination of histone H2B by Rad6.* J Biol Chem, 2002. **277**(32): p. 28368-71.
10. Kim, T. and S. Buratowski, *Dimethylation of H3K4 by Set1 recruits the Set3 histone deacetylase complex to 5' transcribed regions.* Cell, 2009. **137**(2): p. 259-72.
11. Kim, T., et al., *Set3 HDAC mediates effects of overlapping noncoding transcription on gene induction kinetics.* Cell, 2012. **150**(6): p. 1158-69.
12. Kim, J., et al., *RAD6-Mediated transcription-coupled H2B ubiquitylation directly stimulates H3K4 methylation in human cells.* Cell, 2009. **137**(3): p. 459-71.
13. Hwang, W.W., et al., *A conserved RING finger protein required for histone H2B monoubiquitination and cell size control.* Mol Cell, 2003. **11**(1): p. 261-6.
14. Robzyk, K., J. Recht, and M.A. Osley, *Rad6-dependent ubiquitination of histone H2B in yeast.* Science, 2000. **287**(5452): p. 501-4.
15. Wood, A., et al., *Bre1, an E3 ubiquitin ligase required for recruitment and substrate selection of Rad6 at a promoter.* Mol Cell, 2003. **11**(1): p. 267-74.
16. Krogan, N.J., et al., *The Paf1 complex is required for histone H3 methylation by COMPASS and Dot1p: linking transcriptional elongation to histone methylation.* Mol Cell, 2003. **11**(3): p. 721-9.

466 17. Ng, H.H., S. Dole, and K. Struhl, *The Rtf1 component of the Paf1*
467 *transcriptional elongation complex is required for ubiquitination of histone*
468 *H2B.* J Biol Chem, 2003. **278**(36): p. 33625-8.
469 18. Van Oss, S.B., et al., *The Histone Modification Domain of Paf1 Complex*
470 *Subunit Rtf1 Directly Stimulates H2B Ubiquitylation through an Interaction*
471 *with Rad6.* Mol Cell, 2016. **64**(4): p. 815-825.
472 19. Wood, A., et al., *The Paf1 complex is essential for histone monoubiquitination*
473 *by the Rad6-Bre1 complex, which signals for histone methylation by COMPASS*
474 *and Dot1p.* J Biol Chem, 2003. **278**(37): p. 34739-42.
475 20. Francette, A.M., S.A. Tripplehorn, and K.M. Arndt, *The Paf1 Complex: A*
476 *Keystone of Nuclear Regulation Operating at the Interface of Transcription and*
477 *Chromatin.* J Mol Biol, 2021. **433**(14): p. 166979.
478 21. Jaehning, J.A., *The Paf1 complex: platform or player in RNA polymerase II*
479 *transcription?* Biochim Biophys Acta, 2010. **1799**(5-6): p. 379-88.
480 22. Squazzo, S.L., et al., *The Paf1 complex physically and functionally associates*
481 *with transcription elongation factors in vivo.* Embo j, 2002. **21**(7): p. 1764-74.
482 23. Kim, J., M. Guermah, and R.G. Roeder, *The human PAF1 complex acts in*
483 *chromatin transcription elongation both independently and cooperatively with*
484 *SII/TFIIS.* Cell, 2010. **140**(4): p. 491-503.
485 24. Chen, Y., et al., *DSIF, the Paf1 complex, and Tat-SF1 have nonredundant,*
486 *cooperative roles in RNA polymerase II elongation.* Genes Dev, 2009. **23**(23): p.
487 2765-77.
488 25. Mueller, C.L., et al., *The Paf1 complex has functions independent of actively*
489 *transcribing RNA polymerase II.* Mol Cell, 2004. **14**(4): p. 447-56.
490 26. Penheiter, K.L., et al., *A posttranscriptional role for the yeast Paf1-RNA*
491 *polymerase II complex is revealed by identification of primary targets.* Mol Cell,
492 2005. **20**(2): p. 213-23.
493 27. Sheldon, K.E., D.M. Mauger, and K.M. Arndt, *A Requirement for the*
494 *Saccharomyces cerevisiae Paf1 complex in snoRNA 3' end formation.* Mol Cell,
495 2005. **20**(2): p. 225-36.
496 28. Tomson, B.N., et al., *Identification of a role for histone H2B ubiquitylation in*
497 *noncoding RNA 3'-end formation through mutational analysis of Rtf1 in*
498 *Saccharomyces cerevisiae.* Genetics, 2011. **188**(2): p. 273-89.
499 29. Koch, C., et al., *A role for Ctr9p and Paf1p in the regulation G1 cyclin*
500 *expression in yeast.* Nucleic Acids Res, 1999. **27**(10): p. 2126-34.
501 30. Mueller, C.L. and J.A. Jaehning, *Ctr9, Rtf1, and Leo1 are components of the*
502 *Paf1/RNA polymerase II complex.* Mol Cell Biol, 2002. **22**(7): p. 1971-80.
503 31. Costa, P.J. and K.M. Arndt, *Synthetic lethal interactions suggest a role for the*
504 *Saccharomyces cerevisiae Rtf1 protein in transcription elongation.* Genetics,
505 2000. **156**(2): p. 535-47.
506 32. Rozenblatt-Rosen, O., et al., *The tumor suppressor Cdc73 functionally*
507 *associates with CPSF and CstF 3' mRNA processing factors.* Proc Natl Acad Sci
508 U S A, 2009. **106**(3): p. 755-60.
509 33. Chu, X., et al., *Structural insights into Paf1 complex assembly and histone*
510 *binding.* Nucleic Acids Res, 2013. **41**(22): p. 10619-29.
511 34. Zhu, B., et al., *The human PAF complex coordinates transcription with events*
512 *downstream of RNA synthesis.* Genes Dev, 2005. **19**(14): p. 1668-73.
513 35. Zhao, Y., et al., *Cryptococcus neoformans, a global threat to human health.*
514 Infect Dis Poverty, 2023. **12**(1): p. 20.

515 36. May, R.C., et al., *Cryptococcus: from environmental saprophyte to global*
516 *pathogen.* Nat Rev Microbiol, 2016. **14**(2): p. 106-17.
517 37. Rajasingham, R., et al., *The global burden of HIV-associated cryptococcal*
518 *infection in adults in 2020: a modelling analysis.* Lancet Infect Dis, 2022.
519 **22**(12): p. 1748-1755.
520 38. Iyer, K.R., et al., *Treatment strategies for cryptococcal infection: challenges,*
521 *advances and future outlook.* Nature Reviews Microbiology, 2021. **19**(7): p.
522 454-466.
523 39. Zhao, Y., et al., *Life Cycle of Cryptococcus neoformans.* Annu Rev Microbiol,
524 2019. **73**: p. 17-42.
525 40. Lin, X. and J. Heitman, *The biology of the Cryptococcus neoformans species*
526 *complex.* Annu Rev Microbiol, 2006. **60**: p. 69-105.
527 41. Liu, R., et al., *The COMPASS Complex Regulates Fungal Development and*
528 *Virulence through Histone Crosstalk in the Fungal Pathogen Cryptococcus*
529 *neoformans.* J Fungi (Basel), 2023. **9**(6).
530 42. Fan, Y. and X. Lin, *Multiple Applications of a Transient CRISPR-Cas9 Coupled*
531 *with Electroporation (TRACE) System in the Cryptococcus neoformans Species*
532 *Complex.* Genetics, 2018. **208**(4): p. 1357-1372.
533 43. Lin, J., Y. Fan, and X. Lin, *Transformation of Cryptococcus neoformans by*
534 *electroporation using a transient CRISPR-Cas9 expression (TRACE) system.*
535 Fungal Genet Biol, 2020. **138**: p. 103364.
536 44. Xia, Y., et al., *T5 exonuclease-dependent assembly offers a low-cost method for*
537 *efficient cloning and site-directed mutagenesis.* Nucleic Acids Res, 2019. **47**(3):
538 p. e15.
539 45. Fan, Y. and X. Lin, *An intergenic "safe haven" region in Cryptococcus*
540 *neoformans serotype D genomes.* Fungal Genet Biol, 2020. **144**: p. 103464.
541 46. Upadhya, R., et al., *A fluorogenic C. neoformans reporter strain with a robust*
542 *expression of m-cherry expressed from a safe haven site in the genome.* Fungal
543 Genet Biol, 2017. **108**: p. 13-25.
544 47. Zhao, Y. and X. Lin, *A PAS Protein Directs Metabolic Reprogramming during*
545 *Cryptococcal Adaptation to Hypoxia.* mBio, 2021. **12**(2).
546 48. Vartivarian, S.E., et al., *Regulation of cryptococcal capsular polysaccharide by*
547 *iron.* J Infect Dis, 1993. **167**(1): p. 186-90.
548 49. Lin, J., et al., *Immunoprotection against Cryptococcosis Offered by Znf2*
549 *Depends on Capsule and the Hyphal Morphology.* mBio, 2022. **13**(1): p.
550 e0278521.
551 50. Zhao, Y., et al., *Activation of Meiotic Genes Mediates Ploidy Reduction during*
552 *Cryptococcal Infection.* Curr Biol, 2020. **30**(8): p. 1387-1396.e5.
553 51. Zhai, B., et al., *Congenic strains of the filamentous form of Cryptococcus*
554 *neoformans for studies of fungal morphogenesis and virulence.* Infect Immun,
555 2013. **81**(7): p. 2626-37.
556 52. Zhao, Y., S. Upadhyay, and X. Lin, *PAS Domain Protein Pas3 Interacts with*
557 *the Chromatin Modifier Bre1 in Regulating Cryptococcal Morphogenesis.*
558 mBio, 2018. **9**(6).
559 53. Francette, A.M., S.A. Tripplehorn, and K.M. Arndt, *The Paf1 Complex: A*
560 *Keystone of Nuclear Regulation Operating at the Interface of Transcription and*
561 *Chromatin.* Journal of Molecular Biology, 2021. **433**(14).
562 54. Hsueh, Y.P. and W.C. Shen, *A homolog of Ste6, the a-factor transporter in*
563 *Saccharomyces cerevisiae, is required for mating but not for monokaryotic*
564 *fruiting in Cryptococcus neoformans.* Eukaryot Cell, 2005. **4**(1): p. 147-55.

565 55. Wang, P. and J. Heitman, *Signal transduction cascades regulating mating,*
566 *filamentation, and virulence in Cryptococcus neoformans.* Curr Opin Microbiol,
567 1999. **2**(4): p. 358-62.
568 56. Shen, W.C., et al., *Pheromones stimulate mating and differentiation via*
569 *paracrine and autocrine signaling in Cryptococcus neoformans.* Eukaryot Cell,
570 2002. **1**(3): p. 366-77.
571 57. Lin, X., et al., *Transcription factors Mat2 and Znf2 operate cellular circuits*
572 *orchestrating opposite- and same-sex mating in Cryptococcus neoformans.*
573 PLoS Genet, 2010. **6**(5): p. e1000953.
574 58. Wang, L., et al., *Fungal adhesion protein guides community behaviors and*
575 *autoinduction in a paracrine manner.* Proc Natl Acad Sci U S A, 2013. **110**(28):
576 p. 11571-6.
577 59. Chen, S.Y., et al., *Optogenetic Control Reveals Differential Promoter*
578 *Interpretation of Transcription Factor Nuclear Translocation Dynamics.* Cell
579 Syst, 2020. **11**(4): p. 336-353.e24.
580 60. Heximer, S.P., et al., *Mechanisms governing subcellular localization and*
581 *function of human RGS2.* J Biol Chem, 2001. **276**(17): p. 14195-203.
582 61. Vos, S.M., et al., *Structure of activated transcription complex Pol II-DSIF-PAF-*
583 *SPT6.* Nature, 2018. **560**(7720): p. 607-612.
584 62. de Jong, R.N., et al., *Structure and DNA binding of the human Rtf1 Plus3*
585 *domain.* Structure, 2008. **16**(1): p. 149-59.

586

587 **Figure 1. Rtf1 regulates cryptococcal bisexual mating by facilitating H2Bub1 via**
588 **the HMD domain.** (A) Immunoblot analysis of H2Bub1 in *C. deneoformans* wild-type
589 XL280, *rtf1*Δ, and *rtf1*Δ/RTF1 strains. (B) Immunoblot analysis of H3K4me (including
590 H3K4me1, H3K4me2, and H3K4me3) in *C. deneoformans* wild-type XL280, *rtf1*Δ, and
591 *rtf1*Δ/RTF1 strains. (C) Colony morphology of cells during bisexual mating between
592 indicated strains. The same volume of cells with opposite mating type at OD_{600} = 3 were
593 mixed, and 3 μL of mixtures were spotted and cultured on V8 media for 2 days at room
594 temperature in dark. (D) Schematic diagram of pheromone-dependent signaling
595 pathway and transcript levels of genes involved in pheromone signaling. The mating
596 cells were prepared and cultured on V8 media following the same protocol as the
597 colony morphology assay. After 24 h, cells were collected for total RNA extraction and
598 qPCR. (E) Domain structure of Rtf1 homologs in indicated eukaryotes. Cn, *C.*
599 *deneoformans*, Ca, *Candida albicans*, Af, *Aspergillus fumigatus*, Fg, *Fusarium*
600 *graminearum*, Nc, *Neurospora crassa*, Sp, *Schizosaccharomyces pombe*, Sc, *S.*
601 *cerevisiae*, Dm, *Drosophila melanogaster*, Hs, *Homo sapiens*. (F and G) Neighbor-
602 joining tree of Rtf1 homologs and their corresponding HMD in indicated eukaryotes.
603 (H) Schematic diagram of overexpressing constructs of Rtf1, HMD domain, and Plus3
604 domain. The constitutive promoter of *TEF1* gene was used to drive gene expression. (I)
605 Immunoblot analysis of H2Bub1 in strains expressing the indicated proteins. (J)
606 Unisexual hyphal formation of indicated strains on V8 media.

607 **Figure 2. The expression of HMD domain alone rescues the downregulation of**
608 **genes involved in pheromone signaling and filamentous growth due to the deletion**
609 **of *RTF1*.** (A) Volcano plots of differentially expressed genes in *rtf1*Δ, *rtf1*Δ/HMD, and
610 *rtf1*Δ/Plus3 relative to wild-type XL280, respectively, during unisexual mating on V8
611 media. Genes involved in pheromone signaling and filamentous growth were indicated.
612 (B) Reads coverage of indicated gene loci in XL280, *rtf1*Δ, *rtf1*Δ/HMD, and
613 *rtf1*Δ/Plus3 strains. Reads coverage at *TEF1* locus served as control. (C) qPCR
614 quantification of transcript levels of indicated genes in XL280, *rtf1*Δ, *rtf1*Δ/HMD, and
615 *rtf1*Δ/Plus3 strains cultured on V8. The transcript level of indicated genes were relative
616 to its transcript level in XL280 cells cultured in YPD.

617 **Figure 3. The HMD domain alone is sufficient to facilitate global H2Bub1 and**
618 **restore hyphal formation in *rtf1*Δ strain.** (A) Schematic diagram of constructs
619 expressing mNG-labelled Rtf1 or HMD domain with cell membrane tag (RGS2) or

620 NLS. (B) Fluorescence analysis of sub-cellular localizations of Rtf1 and HMD with
621 RGS2 and NLS. (C) Immunoblot analysis of H2Bub1 and H3K4me in strains
622 expressing the indicated proteins. (D) Colony morphology of indicated strains during
623 unisexual mating on V8. (E) ClustalW multiple amino acid sequence alignment of the
624 HMD domain in the indicated eukaryotes. The E95 and F118 residues in *C.de*
625 *neoformans* were indicated with asterisk and dot, respectively. Cn, *C. deneoformans*,
626 Ca, *Candida albicans*, Af, *Aspergillus fumigatus*, Fg, *Fusarium graminearum*, Nc,
627 *Neurospora crassa*, Sp, *Schizosaccharomyces pombe*, Sc, *S. cerevisiae*, Dm,
628 *Drosophila melanogaster*, Hs, *Homo sapiens*. (F and G) The 3D structure of *C.*
629 *deneoformans* HMD domain predicted by SWISS-MODEL with the 3D structure of *S.*
630 *cerevisiae* HMD domain (5emx) as the template. The conserved E95 residue was
631 indicated in red. (H) Immunoblot analysis of H2Bub1 and H3K4me in strains
632 expressing the indicated proteins. (I) Colony morphology of indicated strains during
633 unisexual mating on V8.

634 **Figure 4. Rtf1 and HMD domain regulate virulence traits in both *C. neoformans***
635 **and *C. deneoformans***. (A) Immunoblot analysis of H2Bub1 and H3K4me in strains
636 expressing the indicated proteins in *C. neoformans* strain background. (B) Thermal
637 tolerance and melanin production in *C. neoformans* strain background under indicated
638 conditions. (C) Capsule production in the indicated *C. neoformans* strains on capsule-
639 inducing media. The non-capsule-producing strain *nrg1*Δ was used as control. (D) The
640 indicated strains in *C. neoformans* background were cultured on capsule-inducing
641 media. Cell body diameter of 50 cells were quantified with ImageJ. (E) The ratio between
642 diameters of capsule layer and cell body of the indicated strains in *C. neoformans*
643 background were quantified. 50 cells for each strain were analysed. (F) Melanin
644 production of indicated strains in *C. deneoformans* background in liquid L-DOPA
645 media were quantified by determining OD_{490}. (G) Capsule production in the indicated
646 *C. deneoformans* strains on capsule-inducing media. (H) The ratio between diameters of
647 capsule layer and cell body of the indicated strains in *C. deneoformans* background were
648 quantified. 50 cells for each strain were analysed.

649 **Figure 5. Rtf1 and HMD domain regulate cryptococcal pathogenicity in murine**
650 **models of cryptococcosis.** (A) Schematic diagram of the intranasal and intravenous
651 infection models of cryptococcosis. The inoculum and time for detecting fungal burden
652 in these two infection models were indicated, respectively. (B) The fungal burden of

653 lungs infected by indicated strains through intranasal infection. (C-F) The fungal burden
654 of lungs, brain, kidney, and spleen infected by indicated strains through intravenous
655 infection. (G) The survival curve of animals infected by indicated strains through
656 intravenous infection. The inoculum was the same as the fungal burden assay for
657 intravenous infection. (H) Schematic diagram of the working model depicting the role
658 of Rtf1 and its HMD domain in regulating fungal morphogenesis in *C. deneoformans*.

659 **Supplementary Figure S1.** (A) *RTF1* gene regulates fungal filamentation in *C.*
660 *deneoformans*. (B) The neighbor-joining tree of Plus3 domain in the indicated
661 eukaryotes. (C) ClustalW multiple amino acid sequence alignment of Plus3 domain in
662 the indicated eukaryotes. Cn, *C. deneoformans*, Ca, *Candida albicans*, Af, *Aspergillus*
663 *fumigatus*, Fg, *Fusarium graminearum*, Nc, *Neurospora crassa*, Sp,
664 *Schizosaccharomyces pombe*, Sc, *S. cerevisiae*, Dm, *Drosophila melanogaster*, Hs,
665 *Homo sapiens*.

666 **Supplementary Figure S2. Overexpression of Plus3 domain alone failed to rescue**
667 **the downregulation of genes enriched in sexual reproduction, pheromone**
668 **signaling, and filamentous growth due to *RTF1* deletion.** (A) Venn diagram of
669 significantly enriched (p-value < 0.05) GO terms of downregulated genes in *rtf1*Δ,
670 *rtf1*Δ/HMD, and *rtf1*Δ/Plus3 relative to the wild-type XL280 strain on V8. (B) The 19
671 GO terms of downregulated genes shared by *rtf1*Δ and *rtf1*Δ/Plus3 strains.

672 **Supplementary Figure S3. HMD domain alone successfully restores the expression**
673 **of *MAT2* and *MFα1* in *rtf1*Δ strain.**

674 **Supplementary Table S1.** Strains, plasmids, primers and antibodies used in this study.

675 **Supplementary Data S1.** List of differentially expressed genes in *rtf1*Δ, *rtf1*Δ/HMD,
676 and *rtf1*Δ/Plus3 relative to the wild-type XL280 strain on V8.

677 **Supplementary Data S2.** Potential interacting proteins with Rtf1, HMD, and Plus3
678 identified by CoIP/MS.

Figure 1

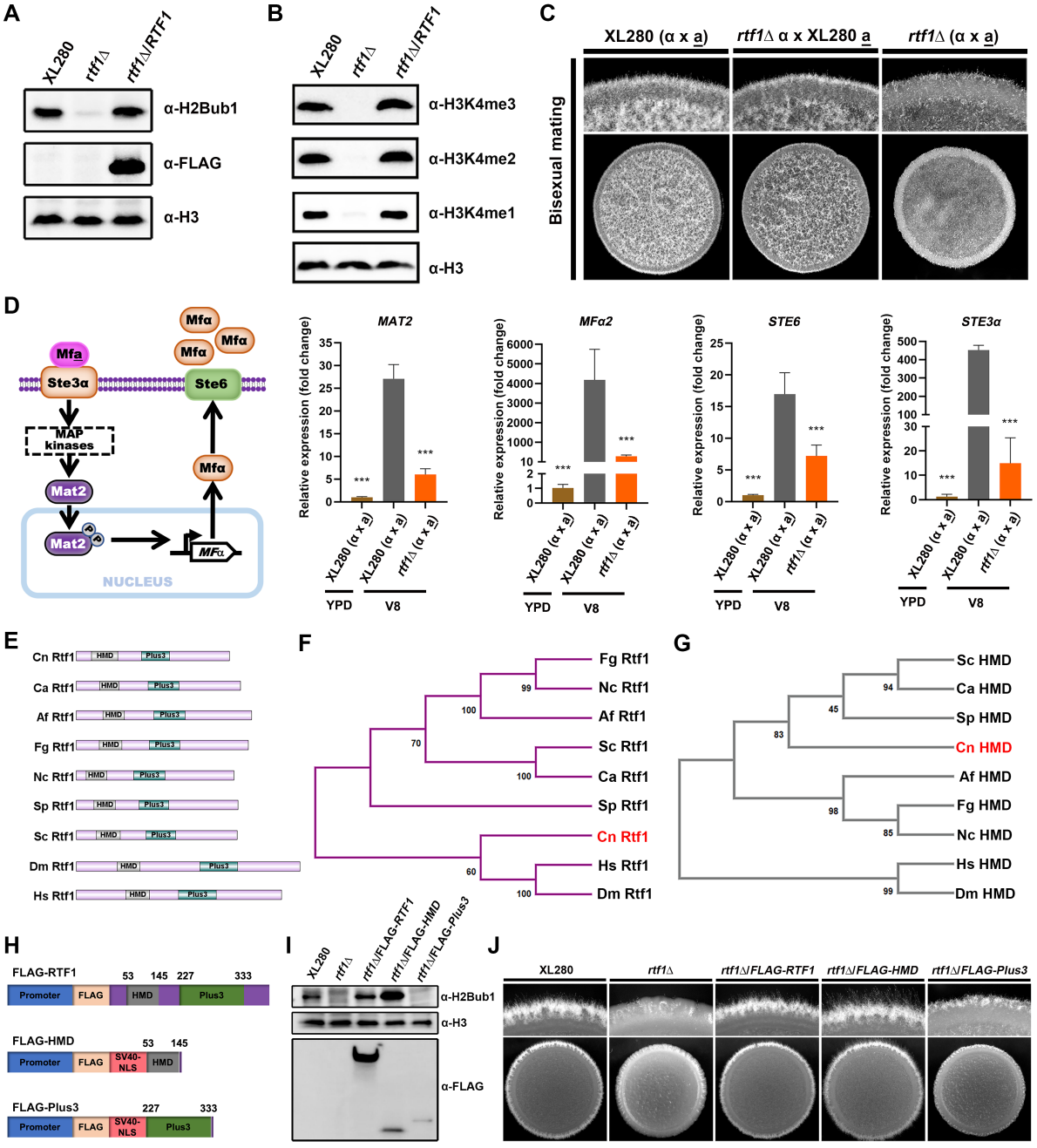
A
XL280
rtf1Δ
rtf1ΔRTF1
α-H2Bub1
α-FLAG
α-H3
B
XL280
rtf1Δ
rtf1ΔRTF1
α-H3K4me3
α-H3K4me2
α-H3K4me1
α-H3
C
XL280 (α x a)
rtf1Δ α x XL280 a
rtf1Δ (α x a)
Bisexual mating
D
Mfa
Mfα
Ste3α
Ste6
MAP kinases
Mat2
NUCLEUS
MFα
MAT2
MFα2
STE6
STE3α
Relative expression (fold change)
XL280 (α x a)
rtf1Δ (α x a)
YPD
V8
E
Cn Rtf1
Ca Rtf1
Af Rtf1
Fg Rtf1
Nc Rtf1
Sp Rtf1
Sc Rtf1
Dm Rtf1
Hs Rtf1
HMD
Plus3
F
Fg Rtf1
Nc Rtf1
Af Rtf1
Sc Rtf1
Ca Rtf1
Sp Rtf1
Cn Rtf1
Hs Rtf1
Dm Rtf1
G
Sc HMD
Ca HMD
Sp HMD
Cn HMD
Af HMD
Fg HMD
Nc HMD
Hs HMD
Dm HMD
H
FLAG-RTF1
53
145
227
333
Promoter
FLAG
HMD
Plus3
FLAG-HMD
SV40-NLS
FLAG-Plus3
I
XL280
rtf1Δ
rtf1ΔFLAG-RTF1
rtf1ΔFLAG-HMD
rtf1ΔFLAG-Plus3
α-H2Bub1
α-H3
α-FLAG
J
XL280
rtf1Δ
rtf1ΔFLAG-RTF1
rtf1ΔFLAG-HMD
rtf1ΔFLAG-Plus3

Figure 2

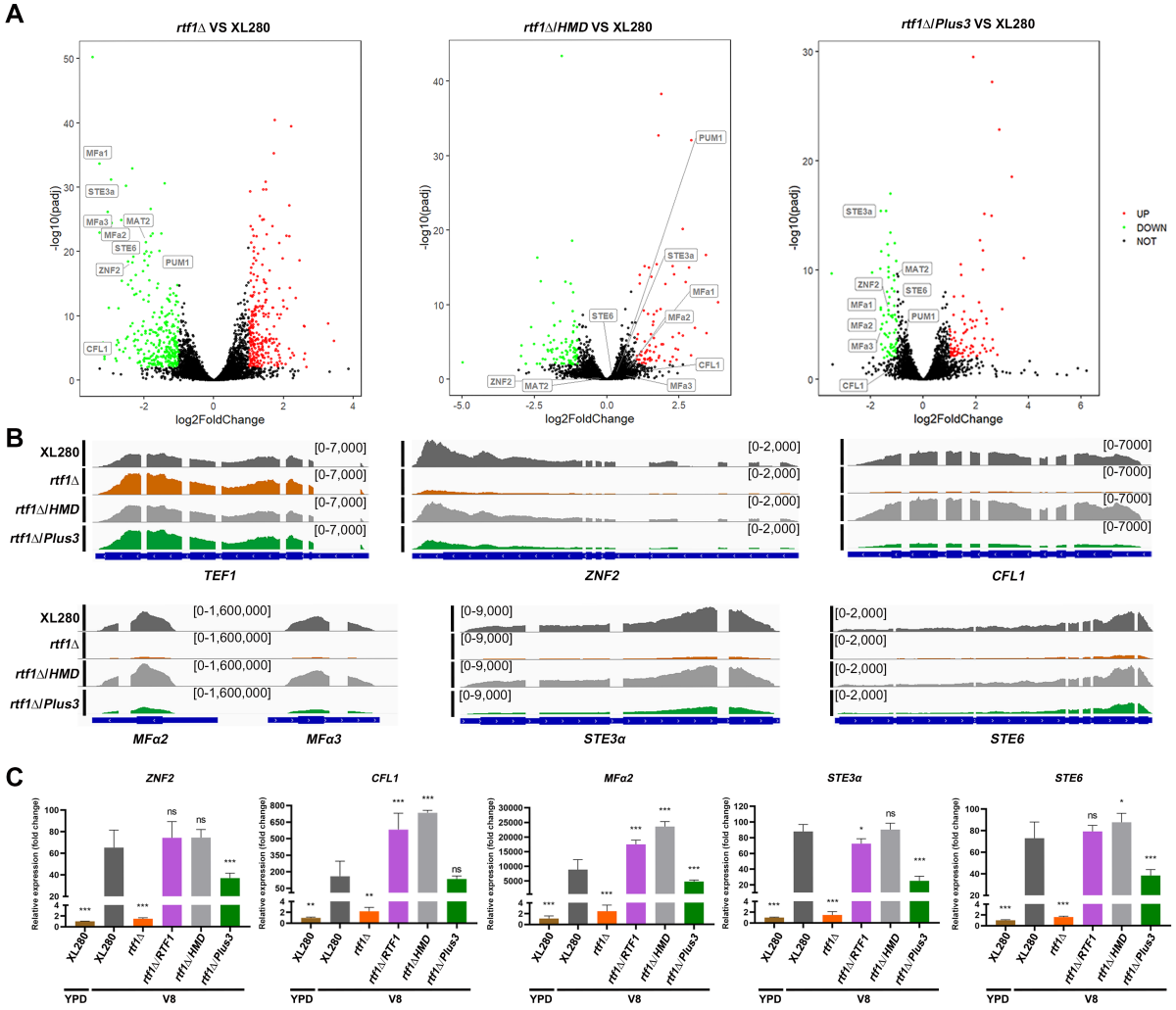
A
rtf1Δ VS XL280
rtf1Δ/HMD VS XL280
rtf1Δ/Plus3 VS XL280
-log10(padj)
log2FoldChange
MFa1
STE3a
MFa3
MAT2
MFa2
STE6
ZNF2
PUM1
CFL1
UP
DOWN
NOT
B
XL280
rtf1Δ
rtf1Δ/HMD
rtf1Δ/Plus3
TEF1
ZNF2
CFL1
MFα2
MFα3
STE3α
STE6
C
Relative expression (fold change)
YPD
V8
XL280
rtf1Δ
rtf1Δ/RTF1
rtf1Δ/HMD
rtf1Δ/Plus3

Figure 3

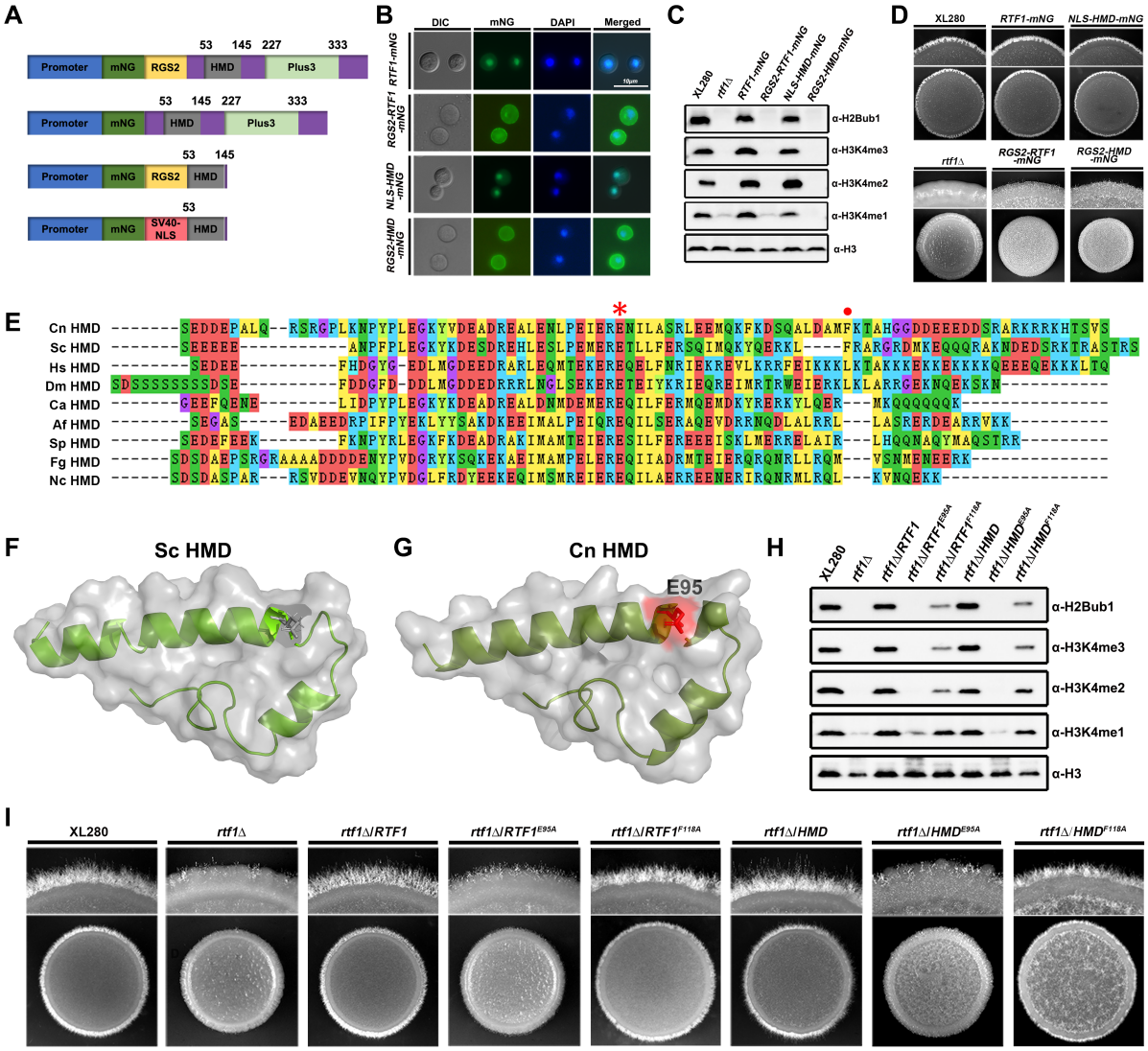
A
Promoter
mNG
RGS2
HMD
Plus3
SV40-NLS
53
145
227
333
B
DIC
mNG
DAPI
Merged
RTF1-mNG
RGS2-RTF1-mNG
NLS-HMD-mNG
RGS2-HMD-mNG
10μm
C
XL280
rtf1Δ
RTF1-mNG
RGS2-RTF1-mNG
NLS-HMD-mNG
RGS2-HMD-mNG
α-H2Bub1
α-H3K4me3
α-H3K4me2
α-H3K4me1
α-H3
D
XL280
RTF1-mNG
NLS-HMD-mNG
rtf1Δ
RGS2-RTF1-mNG
RGS2-HMD-mNG
E
Cn HMD
Sc HMD
Hs HMD
Dm HMD
Ca HMD
Af HMD
Sp HMD
Fg HMD
Nc HMD
F
Sc HMD
G
Cn HMD
E95
H
XL280
rtf1Δ
rtf1ΔRTF1
rtf1ΔRTF1E95A
rtf1ΔRTF1F118A
rtf1ΔHMD
rtf1ΔHMDE95A
rtf1ΔHMDF118A
α-H2Bub1
α-H3K4me3
α-H3K4me2
α-H3K4me1
α-H3
I
XL280
rtf1Δ
rtf1ΔRTF1
rtf1ΔRTF1E95A
rtf1ΔRTF1F118A
rtf1ΔHMD
rtf1ΔHMDE95A
rtf1ΔHMDF118A

Figure 4

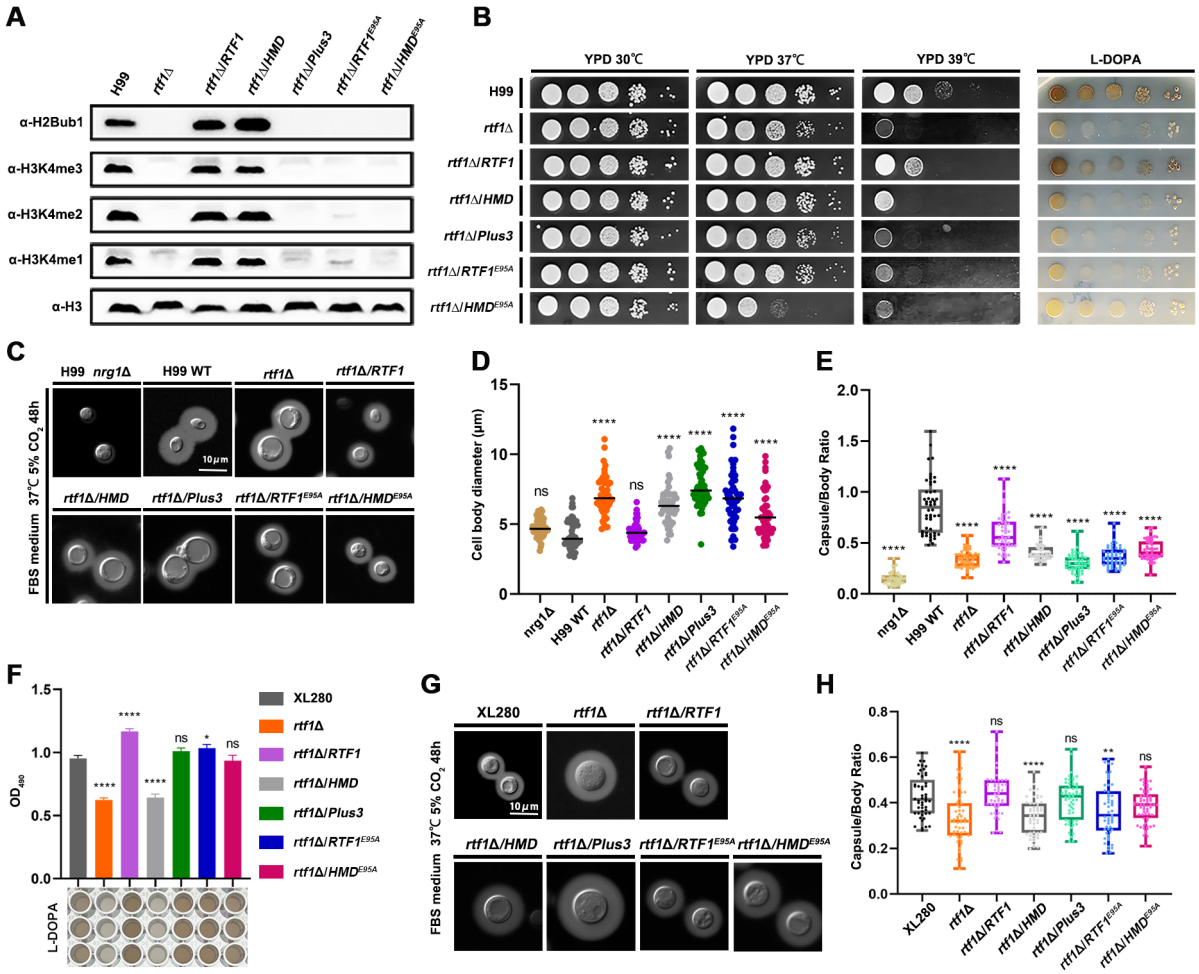
A
H99
rtf1Δ
rtf1Δ/RTF1
rtf1Δ/HMD
rtf1Δ/Plus3
rtf1Δ/RTF1E95A
rtf1Δ/HMDE95A
α-H2Bub1
α-H3K4me3
α-H3K4me2
α-H3K4me1
α-H3
B
YPD 30℃
YPD 37℃
YPD 39℃
L-DOPA
C
H99
nrg1Δ
H99 WT
rtf1Δ
rtf1Δ/RTF1
rtf1Δ/HMD
rtf1Δ/Plus3
rtf1Δ/RTF1E95A
rtf1Δ/HMDE95A
FBS medium 37℃ 5% CO2 48h
10μm
D
Cell body diameter (μm)
ns
****
E
Capsule/Body Ratio
F
OD480
XL280
L-DOPA
G
FBS medium 37℃ 5% CO2 48h
H

Figure 5

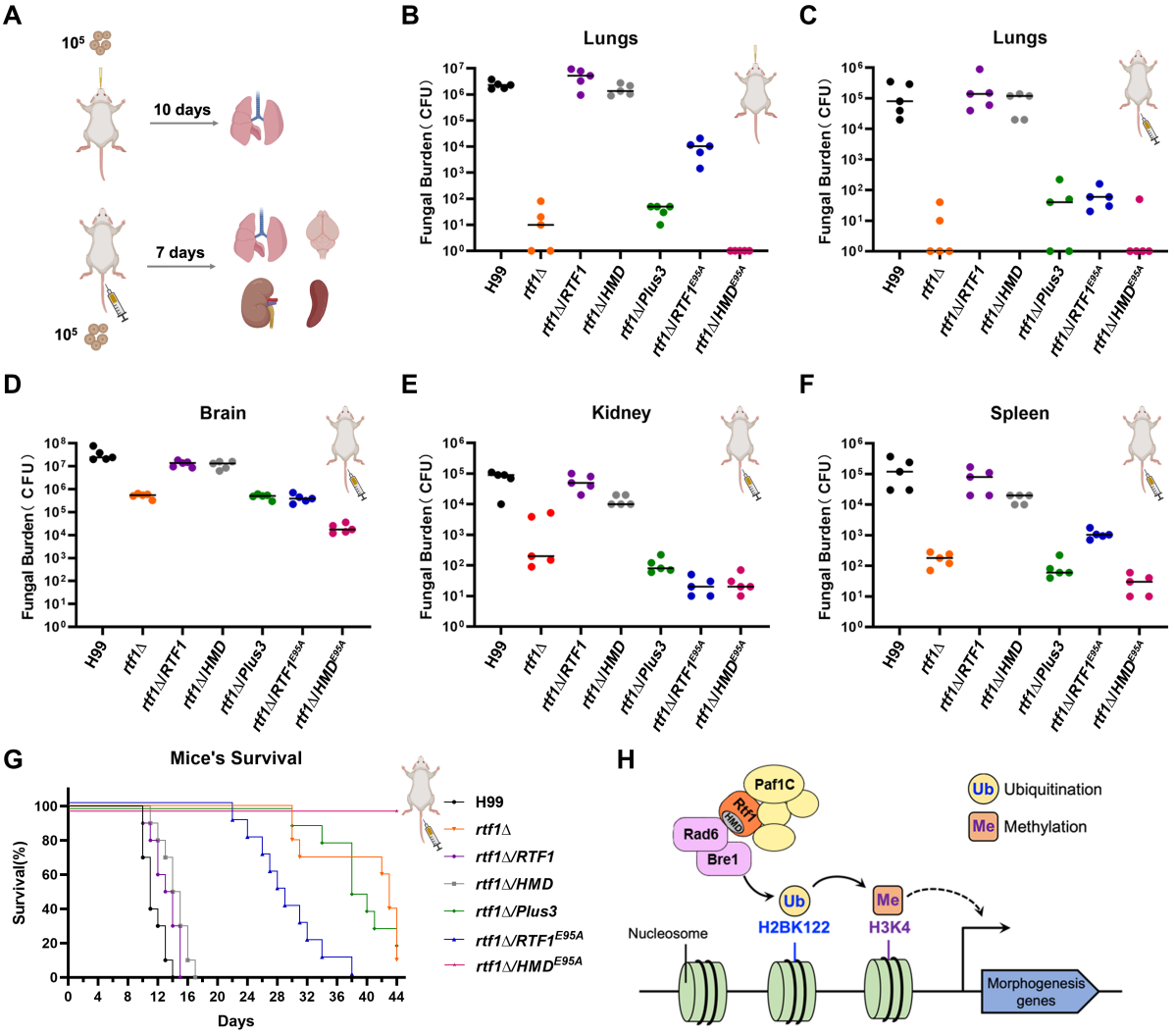
A
10⁵
10 days
7 days
10⁵
B
Lungs
Fungal Burden (CFU)
H99
rtf1Δ
rtf1ΔRTF1
rtf1ΔHMD
rtf1ΔPlus3
rtf1ΔRTF1E95A
rtf1ΔHMDE95A
C
Lungs
D
Brain
E
Kidney
F
Spleen
G
Mice's Survival
Survival(%)
Days
H99
rtf1Δ
rtf1Δ/RTF1
rtf1Δ/HMD
rtf1Δ/Plus3
rtf1Δ/RTF1E95A
rtf1Δ/HMDE95A
H
Paf1C
Rtf1
(HMD)
Rad6
Bre1
Ub
Me
Ubiquitination
Methylation
Nucleosome
H2BK122
H3K4
Morphogenesis genes

Supplementary Figure S1

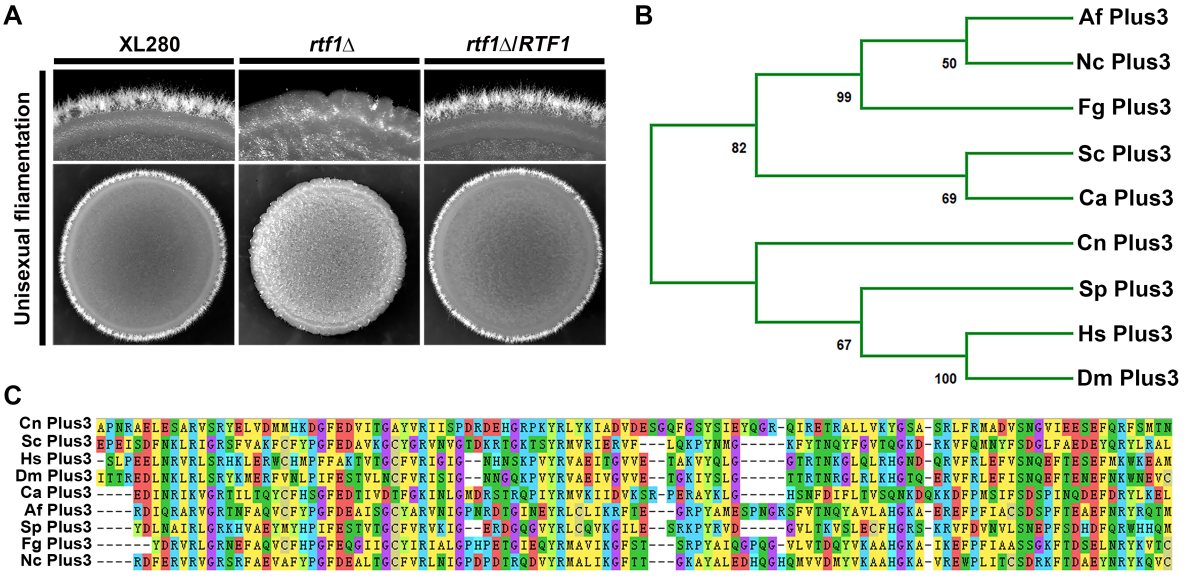

Supplementary Figure S2

A

Enriched GO terms of downregulated genes

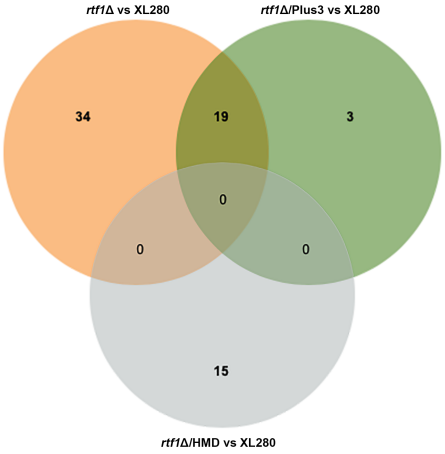

B

19 GO terms of downregulated genes shared by *rtf1*Δ and *rtf1*Δ/Plus3

		*rtf1*Δ vs XL280		*rtf1*Δ/Plus3 vs XL280	
GO ID	GO name	Fold enrichment	*p*-value	Fold enrichment	*p*-value
GO:0019953	sexual reproduction	4.47	1.00E-05	7.13	6.20E-04
GO:0044703	multi-organism reproductive process	4.47	1.00E-05	7.13	6.20E-04
GO:0071444	cellular response to pheromone	10.98	3.92E-05	25.23	1.81E-04
GO:0032005	signal transduction involved in positive regulation of conjugation with cellular fusion	14.64	5.85E-05	42.05	3.13E-05
GO:0000750	pheromone-dependent signal transduction involved in conjugation with cellular fusion	14.64	5.85E-05	42.05	3.13E-05
GO:0019236	response to pheromone	9.99	6.92E-05	22.93	2.47E-04
GO:0040007	growth	4.31	7.80E-05	9.89	2.64E-05
GO:0030447	filamentous growth	4.6	1.05E-04	11.73	9.63E-06
GO:0000749	response to pheromone triggering conjugation with cellular fusion	12.55	1.32E-04	36.04	5.43E-05
GO:0022414	reproductive process	2.92	1.61E-04	4.47	2.09E-03
GO:0000003	reproduction	2.89	1.78E-04	4.43	2.18E-03
GO:0031136	positive regulation of conjugation	10.98	2.54E-04	31.54	8.61E-05
GO:0031139	positive regulation of conjugation with cellular fusion	10.98	2.54E-04	31.54	8.61E-05
GO:2000243	positive regulation of reproductive process	8.79	7.08E-04	25.23	1.81E-04
GO:0046999	regulation of conjugation	7.99	1.07E-03	22.93	2.47E-04
GO:0031137	regulation of conjugation with cellular fusion	7.99	1.07E-03	22.93	2.47E-04
GO:0007618	mating	4.16	1.18E-03	9.09	8.95E-04
GO:2000241	regulation of reproductive process	5.49	1.66E-03	12.61	1.58E-03
GO:0030448	hyphal growth	9.41	2.85E-03	24.03	2.81E-03

Supplementary Figure S3

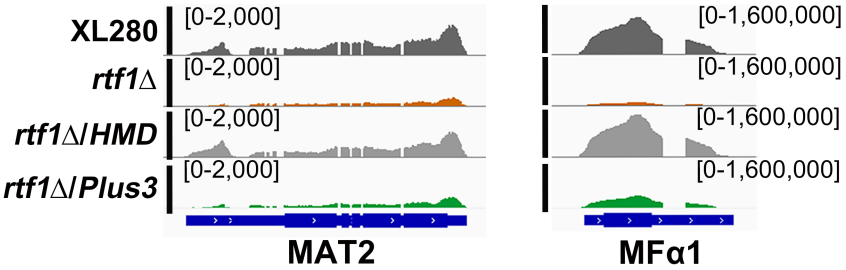

Supplementary Table S1

Strains, plasmids, primers and antibodies used in this study.

Strain name	Genotype	Background	Sources and comments
XL280α	WT	XL280α	[51]
XC27	*rtf1::NAT*	XL280α	This study
XC111	*rtf1::NAT,* P_{CTR4}*-3xFLAG-RTF1-NEO*	XL280α	This study
YJ3	*rtf1::NAT,* P_{TEF1}*-HMD-2xFLAG-HYG*	XL280α	This study
TW3	*rtf1::NAT,* P_{TEF1}*-Plus3-2x FLAG-HYG*	XL280α	This study
YJ53	*rtf1::NAT,* P_{CTR4}*-3xFLAG-RTF1-E95A-NEO*	XL280α	This study
YL27	*rtf1::NAT,* P_{TEF1}*-HMD-E95A-2xFLAG-HYG*	XL280α	This study
YJ55	*rtf1::NAT,* P_{CTR4}*-3xFLAG-RTF1-F118A-NEO*	XL280α	This study
YL30	*rtf1::NAT,* P_{TEF1}*-HMD-F118A-2xFLAG-HYG*	XL280α	This study
YJ70	*rtf1::NAT,*P_{H3}*-RGS2membrane-mNeonGreen-RTF1-NEO*	XL280α	This study
YJ73	*rtf1::NAT,*P_{H3}*-RGS2membrane-mNeonGreen-HMD-NEO*	XL280α	This study
YJ74	*rtf1::NAT,*P_{TEF1}*-RTF1-mNeonGreen-NEO*	XL280α	This study
YJ15	*rtf1::NAT,* P_{TEF1}*-NLS-RTF1-HMD-mNeonGreen-NEO*	XL280α	This study
XL280**a**	WT	XL280**a**	[51]
XC129	*rtf1::NAT*	XL280**a**	This study
H99α	WT	H99α	Lab stock
RL226	*rtf1::NAT*	H99α	Madhani's deletion set
YJ62	*rtf1::NAT,* P_{CTR4}*-3xFLAG-RTF1-NEO*	H99α	This study
YJ64	*rtf1::NAT,* P_{TEF1}*-HMD-2xFLAG-HYG*	H99α	This study
YJ67	*rtf1::NAT,* P_{TEF1}*-Plus3-2xFLAG-HYG*	H99α	This study
YJ78	*rtf1::NAT,* P_{CTR4}*-3xFLAG-RTF1-E95A-NEO*	H99α	This study
YJ82	*rtf1::NAT,* P_{TEF1}*-HMD-E95A-2xFLAG-HYG*	H99α	This study

Plasmid	Genotype	Sources
pYZ175	P_{CTR4}*-3×FLAG-NEO*	This study
pYZ41	P_{TEF1}*-2xFLAG-HYG*	This study
pYZ25	P_{TEF1}*-mNeonGreen-NEO*	This study
pYZ281	P_{CTR4}*-3xFLAG-RTF1-NEO*	This study
pYZ255	P_{TEF1}*-HMD-core-2xFLAG-NEO*	This study
pYZ278	P_{TEF1}*-ATG-NLS-Plus3-2xFLAG-HYG*	This study
pYZ463	P_{CTR4}*-3xFLAG-RTF1-E95A-NEO*	This study
pYZ455	P_{TEF1}*-HMD-E95A-2xFLAG-HYG*	This study
pYZ467	P_{CTR4}*-3xFLAG-RTF1-F118A-NEO*	This study
pYZ459	P_{TEF1}*-HMD-F118A-2xFLAG-HYG*	This study

pYZ317	P_{H3}-*RGS2membrane-mNeonGreen-NEO*	This study
pYZ506	P_{H3}-*RGS2membrane-mNeonGreen-RTF1-NEO*	This study
pYZ509	P_{H3}-*RGS2membrane-mNeonGreen-HMD-NEO*	This study
pYZ554	P_{TEF1}-*RTF1-mNeonGreen-NEO*	This study
pYZ269	P_{TEF1}-*NLS-HMD-mNeonGreen-NEO*	This study

Primer name	**Sequence (5' to 3')**	**Description**
M13F	GTAAAACGACGGCCAGT	NAT/NEO/HYG cassette and TRACE constructs from plasmid
M13R	CAGGAAACAGCTATGAC	NAT/NEO/HYG cassette and TRACE constructs from plasmid
ZhaoLab0003/YZ	TTGGATGCTGGATGCTGGGT	NAT-F
ZhaoLab0004/YZ	CCGTCTTCACCTGCATCTGATT	NAT-split-R
ZhaoLab0015/YZ	TGTGGATGCTGGCGGAGGATA	NAT-split-R for positive PCR of mutant
ZhaoLab0192/YZ	AACTGAGATACCTACAGCGTGAG	gRNA-scaffold-Far-R
ZhaoLab0193/YZ	ACTCCCTGGTCCCATCCCT	CnU6-Far-F
ZhaoLab0011/YZ	CCATCGATTTGCATTAGAACTAAAAACA AAGCA	U6 promoter NF
ZhaoLab0012/YZ	CCGCTCGAGTAAAACAAAAAAGCACCG AC	gRNA scaffold NR
ZhaoLab0054/YZ	GATAGATACTGAGGAGGACAT	PGPD1_F for Cas9
ZhaoLab0055/YZ	GGGCCCCTCTTCACGTGG	TGPD1_R for Cas9
ZhaoLab0013/YZ	AGACTCCACAGCCTAAGATCAACAGTAT ACCCTGCCGGTG	*SH2* gRNA, paired with 0193 (U6 promoter R)
ZhaoLab0014/YZ	GATCTTAGGCTGTGGAGTCTGTTTTAGA GCTAGAAATAGCAAGTT	*SH2* gRNA, paired with 0192 (gRNA scaffold F)
ZhaoLab0105/YZ	GTTCTCTGACCCAAAACATCGTTTTAGA GCTAGAAATAGCAAGTT	*SH3* gRNA, paired with 0193 (U6 promoter R)
ZhaoLab0106/YZ	GATGTTTTGGGTCAGAGAACAACAGTAT ACCCTGCCGGTG	*SH3* gRNA, paired with 0192 (gRNA scaffold F)
ZhaoLab0188/YZ	CGAAGGATGGTTGTCGCTC	screening insertion into SH3 in serotype D
ZhaoLab0189/YZ	GTATCGTCTTGCTCTTCATTCC	screening insertion into SH3 in serotype D
ZhaoLab0190/YZ	GTTGTTTCAGGCCTGCGGATG	screening insertion into SH2 in serotype A
ZhaoLab0191/YZ	GACTCATTCCTATGCCGTTC	screening insertion into SH2 in serotype A
ZhaoLab0044/YZ	TCTGACGCTGCGCCTTTG	*RTF1* deletion in XL280 LF
ZhaoLab0045/YZ	CTGGCCGTCGTTTTACATGGGATGCTG ATGAGATTGCT	*RTF1* deletion in XL280 LR

ZhaoLab0046/YZ	GCTTCGGGCACCACTAAC	*RTF1* deletion in XL280 NLF
ZhaoLab0047/YZ	GTCATAGCTGTTTCCTGGGGAGAAGGATGACTACGA	*RTF1* deletion in XL280 RF
ZhaoLab0048/YZ	AAAGCGAACTGTGGACGA	*RTF1* deletion in XL280 RR
ZhaoLab0049/YZ	GACAAGAAAAGAAACCGA	*RTF1* deletion in XL280 NRR
ZhaoLab0050/YZ	AGCATGGTAGGCCAAAGTACGTTTTAGAGCTAGAAATAGCAAGTT	*RTF1* deletion in XL280 gRNA, paired with 0192 (gRNA scaffold F)
ZhaoLab0051/YZ	GTACTTTGGCCTACCATGCTAACAGTATACCCTGCCGGTG	*RTF1* deletion in XL280 gRNA, paired with 0193 (U6 promoter R)
ZhaoLab0275/YZ	AGAGTGCGAGGGTTAGTAGG	*RTF1* deletion in XL280 Test F
ZhaoLab0276/YZ	GACAAGCAAAGCCCGAGT	*RTF1* deletion in XL280 Test R
ZhaoLab0306/YZ	GTGGCGGTGGGCCGGCCTCTGACCTCGAGAACGAGCTTT	*RTF1* forward with FseI for FLAG tag
ZhaoLab0307/YZ	CTGCTACTGTAACCCTTAATTCAGAAATCTCCCAAATCTAGATCCAGCTG	*RTF1* reverse with PacI for FLAG tag
ZhaoLab0177/YZ	CACAGAAAACTTCAAACCCATGGATAAAGCGGAATTAATTCCCGAGCCTCCAAAAAAGAAGAGAAAGGTCTCTGAAGATGATGAACCAGC	*HMD* forward with FseI for FLAG tag
ZhaoLab0178/YZ	TGCGATCGCGGCCGGCCCGCTCACACTAGTGTGCTTG	*HMD* reverse with SmaI for FLAG tag
ZhaoLab0310/YZ	CACAGAAAACTTCAAACCCATGGATAAAGCGGAATTAATTCCCGAGCCTCCAAAAAAGAAGAGAAAGGTCGCGCCCAACAGGGCCGA	*Plus3* reverse with FseI for FLAG tag
ZhaoLab0311/YZ	TGCGATCGCGGCCGGCCCAGCCTTTATTTCATCGTGCT	*Plus3* reverse with Sma for FLAG tag
ZhaoLab1054/YJ	AGAAAACTTCAAAGGCCGGCCCATGTCTGACCTCGAGAACG	*RTF1* forward with FseI for mNeonGreen tag
ZhaoLab1055/YJ	CCCTTGGACACCATTGCGATGAAATCTCCCAAATCTAGAT	*RTF1* reverse with AsisI for mNeonGreen tag
ZhaoLab0267/YZ	AAACTTCAAAGGCCGGATGGATAAAGCGGAATTAATTCCCGAGCCTCC	*HMD* forward with FseI for mNeonGreen tag
ZhaoLab0268/YZ	TGGACACCATTGCGATCGCGCTCACACTAGTGTGCT	*HMD* reverse with AsisI for mNeonGreen tag
ZhaoLab0315/YZ	CTCGGTACCCGGGGCGGCCGCGAGCTCGGCAGATACGATATGTTG	RGS2membrane Forward with NotI for mNeonGreen tag
ZhaoLab0316/YJ	TGGACACCATGGGCCCAGAACCACTTCCGCCCGA	RGS2membrane reverse with ApaI for mNeonGreen tag
ZhaoLab1047/YJ	CGGTGGCTCTGGGCCGGCCAGGAGCATGATCCGATACAT	*RTF1* forward with FseI for RGS2-mNeonGreen tag
ZhaoLab1048/YJ	CTGCTACTGTAACCCTTAATTAAGAAAT	*RTF1* reverse with AsisI

	CTCCCAAATCTAG	for RGS2-mNeonGreen tag
ZhaoLab1049/YJ	GCTACTGTAACCCTTAATTAAGCTCACACTAGTGTGCTTG	*HMD* reverse with AsisI for mNeonGreen tag
ZhaoLab0872/YJ	GGAAATCGAGAGAGCAAACATCTTGGCGT	Primer for RTF1^{E95A} (GAA-GCA)
ZhaoLab0873/YJ	ACGCCAAGATGTTTGCTCTCTCGATTTCC	Primer for RTF1^{E95A} (GAA-GCA)
ZhaoLab0874/YJ	AGCGCTTGATGCGATGGCCAAGACTGCTCATGGT	Primer for RTF1^{F118A} (UUC-GCC)
ZhaoLab0875/YJ	ACCATGAGCAGTCTTGGCCATCGCATCAAGCGCT	Primer for RTF1^{F118A} (UUC-GCC)
ZhaoLab0823/SW	TTGGAAAGTGCGAGGGTT	*RTF1* deletion in H99 Test F
ZhaoLab0824/SW	GATTATGTCGGAGTTGAGC	*RTF1* deletion in H99 Test R
ZhaoLab0792/RL	CTCTGGTTGGCACGGTG	*real time primer for testing JEC21 DNase effect*
ZhaoLab0793/RL	CGTCGGTCAATCTTCTCG	*real time primer for testing JEC21 DNase effect*
ZhaoLab0794/RL	CGTCACCACTGAAGTCAAGT	*TEF1 real time primer*
ZhaoLab0795/RL	AGAAGCAGCCTCCATAGG	*TEF1 real time primer*
ZhaoLab0593/YJ	AATGGTGGCACGAACGATCT	*CFL1 real time primer*
ZhaoLab0594/YJ	GTTGTCGCAATCGGGTTCAG	*CFL1 real time primer*
ZhaoLab0595/YJ	GTGATGACGACAAGGAGGCTGTT	*FAD1 real time primer*
ZhaoLab0596/YJ	GAGACGCCAGGGATGTTGATGAA	*FAD1 real time primer*
ZhaoLab0599/YJ	CAGGGTTGTAAGTTCGTTCG	*FAS1 real time primer*
ZhaoLab0600/YJ	TCGCGACTCCTCGAAAT	*FAS1 real time primer*
ZhaoLab0605/YJ	GCCATCTTACCCCTACCATCTAC	*ZNF2 real time primer*
ZhaoLab0606/YJ	TGGACATAGGAACGCTGACAAT	*ZNF2 real time primer*
ZhaoLab0601/YJ	TAGCGGAGCGGACTGGAAAGA	*STE3alpha real time primer*
ZhaoLab0602/YJ	CTCGACCGAGACGGCAATCATTA	*STE3alpha real time primer*
ZhaoLab0603/YJ	GCGAATCCACCACCGAATCAATC	*STE6 real time primer*
ZhaoLab0604/YJ	CGACGACTGCAACGCACTCT	*STE6 real time primer*
ZhaoLab0607/YJ	ATCTTCACCACCTTCACTTCT	*MFalpha2 real time primer*
ZhaoLab0608/YJ	CTAGGCGATGACACAAAGG	*MFalpha2 real time primer*
ZhaoLab1252/YJ	GCTCCTCGCTACATCTCCTCA	*MAT2 real time primer F*
ZhaoLab1253/YJ	TGTTTCGGTCTACGATACCAGTT	*MAT2 real time primer R*
ZhaoLab1254/YJ	TTGTTGGAGGATTTCAGGTTGA	*PUM1 real time primer F*
ZhaoLab1255/YJ	GTCTTCAGGAGTGGCGGTTT	*PUM1 real time primer R*

Antibody	Item number	Dilution	Brand
Ubiquityl-Histone H2B-K120 Rabbit mAb	5546T	1:1000	Cell signaling
TriMethyl-Histone H3-K4 Rabbit pAb	A2357	1:2000	ABclonal
DiMethyl-Histone H3-K4 Rabbit pAb	A2356	1:2000	ABclonal
MonoMethyl-Histone H3-K4 Rabbit pAb	A2355	1:2000	ABclonal
Histone H3 Rabbit pAb	A2348	1:5000	ImmunoWay
Flag-Tag Mouse mAb	AB0008	1:2000	Abways
Goat Anti-Mouse	RS0001	1:20000	ImmunoWay
Goat Anti-Rabbit	RS0002	1:20000	ImmunoWay